Automatic Detection of Choroidal Hyperpermeability using Machine Learning Strategies

João Geraldes Salgueiro

Joao.g.salgueiro@tecnico.ulisboa.pt

Instituto Superior Técnico, Lisboa, Portugal

November 2023

Abstract

Machine Learning techniques based on deep neural semantic models have been successfully used in multiple biomedical imaging challenges. In this study, we present a new approach for the Automatic Detection of Choroidal Hyperpermeability points, on patients with Central Serous Chorioretinopathy, using Optical Coherence Tomography. This work focuses on developing an automatic pipeline that leverages machine learning techniques to generate two essential artifacts: a thickness map and a binary classification indicating the presence of choroidal hyperpermeability points. Using the connection between abnormal choroidal thickness and patterns and the presence of choroidal hyperpermeability points, our methodology uses the generated choroidal thickness maps to provide an automatic detection of choroidal hyperpermeability points. The practical application of this project is demonstrated in the context of central serous chorioretinopathy (CSCR), a condition where the automatic detection of choroidal hyperpermeability holds clinical significance. The proposed automatic pipeline has the potential to enhance diagnostic processes for CSCR, providing a more efficient and reliable method for identifying choroidal hyperpermeability points in OCT scans. Using this methodology, we achieved results of 94.46% Dice score in choroidal segmentation challenge and a classification accuracy of 81,25% of the presence of choroidal hyperpermeability points.

Keywords: Machine Learning, Ophthalmology, OCT, Choroid, Semantic Segmentation, CSCR

1. Introduction

Central Serous Chorioretinopathy (CSCR) is a retinal disorder characterized by the accumulation of fluid in the subretinal space, leading to vision impairment[1]. Early and accurate diagnosis of Choroidal Hyperpermeability (CH), a key hallmark of CSCR, is critical for effective treatment and patient care. In recent years, advancements in medical imaging and machine learning techniques have opened new avenues for improving the diagnostic process[2].

This work presents a comprehensive exploration into the realm of machine learning techniques, specifically Convolutional Neural Networks (CNNs) and U-Net segmentation, applied to Optical Coherence Tomography (OCT) scans with a focus on the automatic detection and classification of CH points within choroidal thickness maps. This research aims to bridge the gap between cutting-edge technology and clinical practice, helping healthcare professionals with a robust non-invasive tool for early CSCR detection.

1.1 Human Eye, the choroid, and its impact on retinal health

The human eye is a complex structure with two main areas: the anterior (front) and posterior (back) zones, as demonstrated in Figure 1. In the posterior zone, the retina plays a vital role in processing light signals for the brain. It relies on the choroid, a vascular layer between the retina and the sclera, to supply essential nutrients and oxygen[3–5]. The choroid contains a network of blood vessels, including the choriocapillaris, which transport vital elements to the retina and remove metabolic waste. Additionally, the choroid helps regulate the

intraocular pressure (IOP) and control blood flow in the ciliary body. While the choroid's functions may not be directly related to vision, they are crucial for overall eye health, especially to the retina. Any issues in the choroid might lead to oxygen deficiency, potentially causing damage to the retina and contributing to various eye conditions[3,4,7].

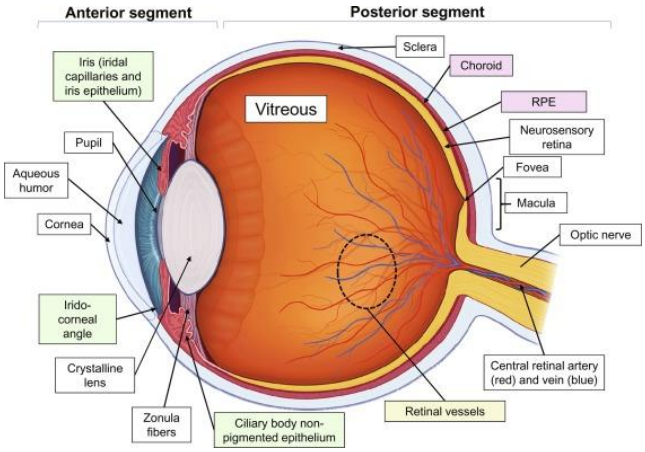

Figure 1: Schematic illustration of Laser Photocoagulation treatment for CSCR[6]

1.2 Choroidal Hyperpermeability as a biomarker of Central Serous Chorioretinopathy

CSCR is a retinal disorder characterized by the accumulation of subretinal fluid, primarily in the macula, a region responsible for central vision[1]. This fluid accumulation, often resulting from disruptions in the retinal pigment epithelium (RPE)[8], can lead to vision loss. Risk factors such as stress and hormonal imbalances, particularly high levels of glucocorticoids, have been associated with CSCR. Symptoms include reduced visual accuracy, blurred central vision, and color differentiation difficulties.

While most cases resolve spontaneously, some require intervention to reduce fluid accumulation and aid RPE recovery. Treatment options include lifestyle modifications and laser photocoagulation, although the latter carries risks and must be carefully considered by clinicians[1,9].

Identifying CSCR biomarkers has been challenging, but recent advances in biomedical imaging techniques have led to breakthroughs. Abnormalities in choroidal thickness and vascularity have emerged as potential biomarkers. Dilated choroidal vessels, enlarged vortex vein ampullae, imbalanced choroidal venous drainage, and disrupted intervortex anastomoses are among the markers that can aid in diagnosis and treatment decision-making[10,11].

A point of hyperpermeability in the context of CSCR refers to a specific area in the choroid where the blood vessels exhibit increased permeability. This heightened permeability allows fluids, such as plasma and proteins, to leak into the surrounding tissues, including the subretinal space (Figure 2)[2].

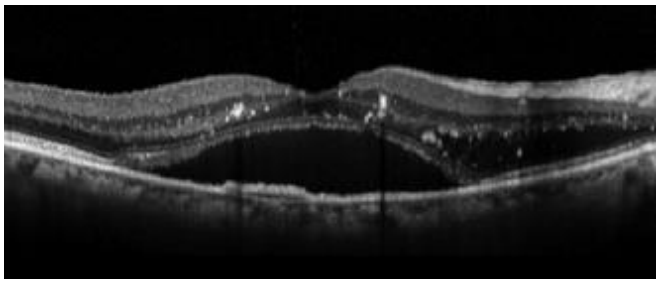

Figure 2*:* Horizontal sectional image of serous detachment of the retina[12]

Such points of hyperpermeability are considered biomarkers because their presence or alteration can provide valuable insights into the pathophysiology of CSCR[2]. Detecting these biomarkers through imaging techniques can aid in the diagnosis of CSCR and guide treatment decisions, offering clinicians a more precise understanding of the disease and its progression within the eye. To effectively identify these biomarkers and provide accurate diagnoses, clinicians rely on in vivo imaging techniques. These techniques allow real-time visualization of internal processes and structures, enabling precise evaluation of anatomical changes and facilitating optimal treatment strategies for CSCR patients.

1.3 Indocyanine Green Angiography

Indocyanine Green Angiography (ICGA) has emerged as the gold-standard in ophthalmology for *in vivo* imaging of the choroid[13]. This imaging protocol involves the injection of a water-soluble dye called Indocyanine Green (ICG). ICG is known for its exceptional fluorescent properties, particularly in the near-infrared spectrum, making it ideal for imaging deep tissues like the choroid located beneath the retina and Bruch's Membrane (BM)[13–15]. During an ICGA procedure, a small amount of ICG dye is intravenously injected, and it quickly mixes with plasma and proteins. The dye circulates through the choroidal arteries and

choriocapillaris, absorbing and re-emitting near-infrared light, which specialized cameras capture to create *in vivo* images of choroidal vasculature. This imaging technique provides a comprehensive view of the choroid's vasculature, unlike other protocols such as Fluorescein Angiography (FA), which primarily focuses on retinal blood vessels[14].

ICGA is the current standard for diagnosing biomarkers and points of choroidal hyperpermeability associated with conditions like Central Serous Chorioretinopathy (CSCR). It offers clear *enface* images of choroidal vasculature, enabling the identification of imbalanced choroidal venous drainage and leak points for guidance on laser treatment (Figure 3).

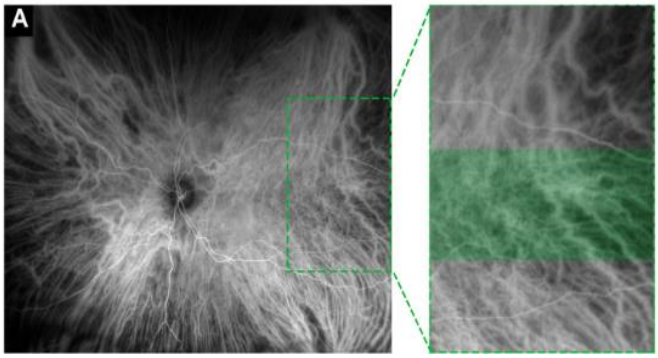

Figure 3 Ultrawide field (UWF) ICGA scan with zoom on pachyvessels[16]

However, ICGA has drawbacks. It is an invasive procedure involving intravenous dye injection, with a rare risk of allergic reactions. It must be performed in a hospital setting with access to emergency care. Patients also need to prepare by discontinuing certain medications and making dietary adjustments. Additionally, ICGA scans can be time-consuming, taking up to 30 minutes. Due to these challenges, there is growing interest in developing non-invasive and more time-efficient alternatives to ICGA[13,14,17].

1.4 Optical Coherence Tomography as a replacement for ICGA scans

Optical Coherence Tomography (OCT), introduced in the 1990s, is a non-invasive imaging technique that has revolutionized the field of biomedical imaging, providing high-resolution, *in vivo* images of biological tissues. Similar to ultrasound imaging, OCT uses light waves instead of sound waves[18,19].

In OCT, a low-coherence light source, typically near-infrared light, is split into two paths: one directed at the tissue being examined, and the other at a reference mirror. When the light interacts with biological tissue, it gets partially absorbed and scattered[19]. The reflected beams from the tissue and the reference arm are then analyzed by a spectrometer, allowing the creation of cross-sectional scans with remarkable detail. OCT offers an image resolution ranging from 1 to 15 µm in both axial and lateral directions. In ophthalmology, OCT scans have become an indispensable tool for *in vivo* imaging of ocular structures, including the retina, optic nerve, choroid, and sclera. Its ability to produce volume scans allows clinicians to visualize cross-sections in multiple axes[18–20].

Although OCT scans do not provide direct vasculature projection, they offer valuable information for clinicians. By processing the data from multiple B-scans, *enface* scans and choroidal thickness maps can be generated, aiding in the diagnosis of conditions like (CSCR). However, this process requires the segmentation of numerous B-scans, making manual segmentation impractical. Therefore, automatic image segmentation methods are essential for efficiently transforming OCT scans into clinically informative images.

In summary, OCT is a powerful and non-invasive imaging technique that provides high-resolution, images of biological tissues, particularly in ophthalmology, where it enables detailed assessment of critical ocular structures and with a particular set of transformations can provide information about the vessel's vasculature and thickness.

1.5 Deep Neural Semantic Segmentation

Neural Networks (NNs) are potent tools in computer vision, especially in tasks like semantic segmentation, where they effectively emulate the neural behavior of the human brain. These networks process and learn from data by employing interconnected nodes, much like neurons in the brain, enabling them to conduct computations and utilize activation functions to grasp intricate relationships within the data[21,22].

In the training of NNs, which entails both forward and backward passes, the objective is to minimize prediction errors using optimization techniques like gradient descent. This training process relies on diverse

loss functions, selected based on the specific problem being addressed. Moreover, factors such as batch size and the number of training epochs play pivotal roles in managing the data used during training, significantly influencing the network's learning performance[22–25].

A specific type of NN known as Convolutional Neural Networks (CNNs) has gained prominence for its exceptional precision in representing visual features. CNNs have become a cornerstone in tasks like semantic segmentation, where they assign distinct categories to each pixel within an image. This remarkable capability has positioned CNNs as the state-of-the-art choice in various domains, including biomedical and ophthalmological imaging, where they play a pivotal role in achieving meticulous image analysis and segmentation[21,26].

1.5.1 U-Net and U-Net++

In 2015, Olaf Ronneberger *et al.* introduced the groundbreaking U-Net architecture, which quickly gained widespread recognition for its exceptional performance in various medical image segmentation tasks, such as breast cancer identification and brain tumor segmentation in MRI scans[26,27]. The U-Net's strength lies in its ability to effectively capture fine image details while preserving spatial information. This architecture comprises two main components: the encoder and the decoder. The encoder extracts high-level features from the input, employing standard CNN layers with multiple convolutional and pooling layers to progressively downsample the spatial dimension while increasing channel count. The decoder then reconstructs the spatial dimension of the feature maps from the encoder, utilizing upsampling layers and skip connections to combine high-level semantic information with finer-grained details from the encoder[26]. The U-Net's unique design forms a U-shaped architecture. A notable advantage of the U-Net architecture is its capability to handle highly imbalanced datasets commonly encountered in medical image segmentation. Through the use of skip connections and up sampling, the network can produce accurate segmentation maps, even for small or underrepresented objects of interest in the training data.

In 2018, Zhou *et al*. sought to further enhance the U-Net's capabilities and introduced an evolutionary architecture called U-Net++. The core concept was to incorporate multiple nested U-Nets, each stacked upon the previous one to progressively capture finer details and contextual information[28]. This hierarchical organization features layers, each consisting of an encoder and decoder, with skip connections receiving inputs from the preceding layer. U-Net++ has been widely adopted in various biomedical image segmentation challenges since its inception, excelling in capturing finer-grained details compared to the standard U-Net architecture[29].

1.5.2 Dilated Residual U-Net

In 2018, Devalla *et al.* introduced a novel variation of the U-Net architecture known as Dilated-Residual U-net (DRUNET). What sets DRUNET apart from the conventional U-Net is its utilization of dilated convolutions. Dilated convolutions enable (CNNs) to have an enhanced receptive field, allowing each neuron to analyze a larger portion of the image by introducing "holes" between the elements of the convolutional kernel[30]. The dilation rate controls the size of these "holes," with larger rates resulting in larger receptive fields. DRUNET also incorporates skip connections to prevent the network from becoming excessively deep and overfitting to the training data. Residual connections, a deep learning technique, enable non-adjacent layers to connect directly to deeper or shallower layers[30].

DRUNET was specifically designed for segmenting the optic nerve head (ONH) in OCT scans, where it demonstrated remarkable performance. It achieved a Dice Coefficient of 0.91, a segmentation metric used for evaluation, outperforming other U-Net variations. In comparison, the best results obtained by alternative methods were around 0.856. This success underscored the potential of DRUNET in accurately segmenting structures from OCT scan images, particularly in the context of ONH segmentation[30].

1.5.3 SegResNet

In 2019, Myronenko *et al.* introduced SegResNet, a type of (CNN) frequently employed in image segmentation tasks. Building upon the ResNet architecture, which utilizes residual connections to address the issue of vanishing gradients, SegResNet was specifically tailored for image segmentation tasks. Similar to DRUNET, SegResNet incorporates dilated convolutions to capture long-range dependencies

within input images and employs skip connections to prevent overfitting[31].

Notably, the SegResNet architecture features an encoder composed of ResNet blocks, each comprising two convolutional layers with a skip connection. Additionally, this architecture often incorporates a variational auto-encoder, a generative model that learns to represent data in a latent space, thereby regularizing the decoder's values. This combination of features makes SegResNet a robust choice for image segmentation tasks, effectively capturing complex image structures while mitigating overfitting concerns[31].

1.5.3 Automatic Image Classification

Automatic Image Classification plays a vital role in computer vision, allowing machines to analyze and categorize image content efficiently. In the field of Biomedical imaging, particularly in Ophthalmology, these techniques are of great importance, aiding physicians in the time-consuming analysis of medical exams. Among the various techniques for automatic image classification, (CNNs) and their variations have become the preferred choice due to their capacity to learn intricate features directly from raw data. CNNs leverage convolutional layers to extract localized features and build hierarchical representations, enabling them to distinguish between different categories and provide accurate classification[32].

Recent findings by Ramtohul *et al.* (2023) have highlighted the correlation between choroidal hyperpermeability and choroidal engorgement points. This work aims to automatically classify generated thickness maps based on the presence of hyperpermeability points. The pipeline's objective is to take in an OCT scan and output a Boolean flag indicating the suspected presence of choroidal hyperpermeability points, thus aiding in medical diagnosis and analysis[16].

2. Related Works

2.1 CNNs in Choroidal Segmentation

In order to obtain any, *enface* information about choroidal vasculature or thickness first there is the need to segment the choroidal layer of tissue in all the B-scans obtained from the cubic OCT scan. This task has its challenges, mostly related to the low contrast in the lower layer, the CSJ. This is due to light refracting upon the upper layer. Some pathologies, like CSCR also exponentiate this problem due to a thickening choroid and vascular dilation[1]. Figure 4 demonstrates that in different areas, red square and green square, of the CSJ the contrast is different due to irregular noise and vessel disposition.

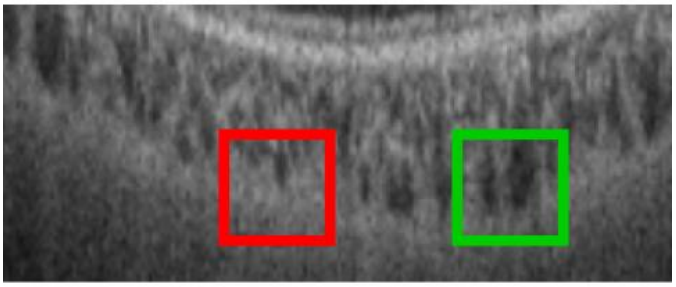

Figure 4. OCT B-scan scaled in the CSJ. The border in the red square has a lot less pixel contrast than the one in the green square

Therefore, for an automatic image segmentation of OCT B-scans there is the need for an innovative approach in order to surpass the hurdles posed by noise and low contrast. Masood *et al* (2019) designed a solution based on a Convolutional Classifier[33]. Firstly, the BM (upper limit) is segmented using a series of structural operations to the image. Then all the pixels above the BM are set to black to minimize the number of classified pixels.

This work chooses to segment the CSJ only and not the choroidal area has a hole. Then the CNN classifier assigns a value for every pixel in the image as in-line or off-line. When classifying each pixel, a patch of the image is used as input, the patch size is very important because it can cause a surplus of information and gravely impact accuracy. The architecture used for the classifier was a pre-trained Cifar-10 model[34].

Additionally, to deal with irregularities in classification a probabilistic model based on distance to other positive pixels was used.
This approach achieved an average dice coefficient of 97%. Although this paper achieved a very good result, it used a large dataset and did not include some denoising technique in it. The accuracy is similar to the

one found in the noise-attenuated images using a simpler architecture. The takeaway is that by using a denoising technique and a more modern encoder decoder based NN better results may be achieved.

2.2 Choroid Segmentation using DRUNET Architecture

Kugelman *et al.* (2018) also tackles this problem of choroidal segmentation and does a comparison between patch-based techniques and semantic segmentation. This study demonstrated that all across the board semantic segmentation performed better than patch-based techniques, achieving a lower average pixel deviation when segmenting the choroid on OCT-scans[35].

2.3 UWF OCT in feature analysis of choroid vasculature

Ramtohul *et al* (2023) set out to discover if salient features in choroidal vasculature can be detected using non-invasive ultrawide field (UWF) OCT scans, thus proposing a substitution method for ICGA scans[16]. In this work, in order to generate the vasculature and *enface* scans a semi-automatic method based on proprietary Canon software and manual adjustments was employed. With this process, this work generated Ultrawide-field *enface* scans of choroidal vascularity, like the one displayed in Figure 5.

Despite not providing any accuracy metrics, this study demonstrates that given a good enough segmentation accuracy, good quality *enface* scans and thickness maps can be generated, thus proving OCT to be a plausible non-invasive alternative to ICGA scans.

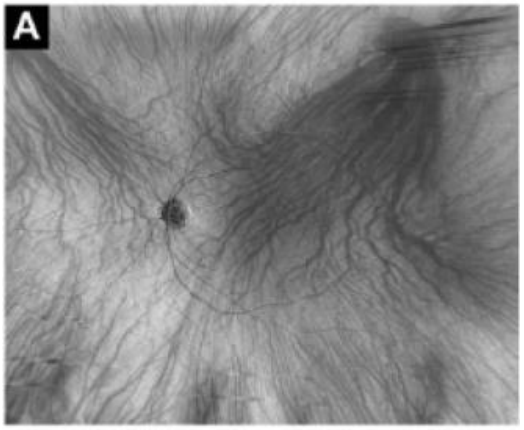

Figure 5: UWF scan of choroidal vasculature from OCT scan.

3. Implementation

3. Proposed Architecture

The main goal of this work is to develop a system capable of accurately detecting choroidal hyperpermeability using OCT scans. There is also the added goal of providing thickness maps as a additional diagnosis tool. The architecture devise with these goals in mind can be divided into two segments. The first where the input cubic OCT scan is sliced alongside the y-axis and transformed into a series of 2-dimensional B-scans. In these individual B-scans the choroid is segmented. Then with some calculations performed a thickness map is generated. The second part of the pipeline intakes the generated thickness maps and classifies them according to having the presence of choroidal hyperpermeability points. Accordingly with the literature, having a accurate enough thickness map should provide enough information to weather the choroid may contain these hyperpermeability points[16]. Figure 6 is a graphical representation of the two sections in the proposed architecture.

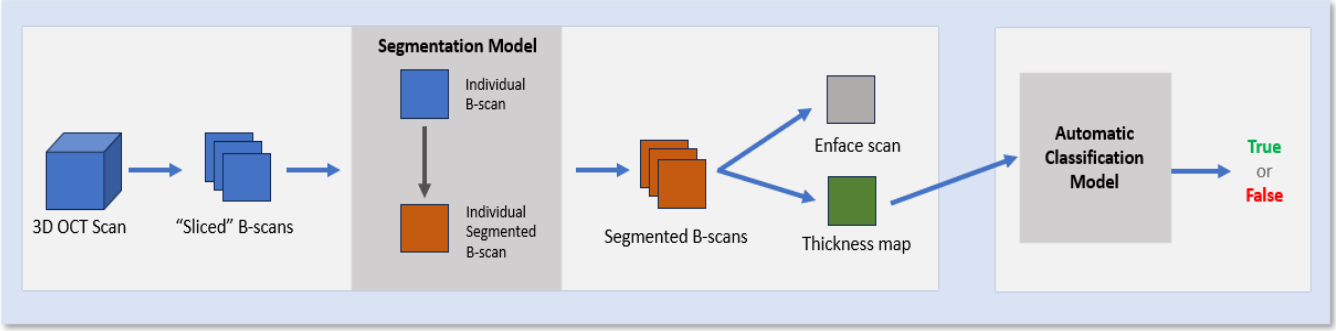

Figure 6 Graphical Representation of the proposed pipeline's architecture

3.2 Choroidal Segmentation

3.2.1 Development

The first component of the general pipeline consists of a segmentation problem. It intakes a 3 dimensional OCT scan and outputs a thickness map. The cube is firstly sliced alongside the y-axis into two dimensional images. In a 15mm by 15mm scan the cube is sliced into 834 individual scans with a width of 834 pixels. Because of the poor quality of the scan around the edges the first 75 and last 75 images are cut from the array of images, leaving us with 684 images.

The images are also trimmed to have a width of 684 pixels. The 684 individual B-scans are then segmented. As previously mentioned, segmenting all the 684 images manually would be too time consuming to be practical, therefore an automatic segmentation model is needed. As referred by study of Kugelman *et al.* (2018) semantic segmentation models are superior to other automatic segmentation techniques driven by artificial intelligence[35].

In this work we sought to find which deep neural sematic segmentation model fits this work better. The models explored were UNET, UNET++, DRUNET and SegResNet[26,28,30,31]. All the models are variations of the famous UNET architecture and were implemented in this work with 3 layered encoder-decoders of 512, 265 and 128 nodes each. The model size was decided taking into consideration the size of the input image (684 by 684 pixels grey scale) and existing hardware limitations. The loss function used was binary-cross entropy (BCE) with logits loss, a popular loss function that has the advantages of fitting better problems where there is only two classes, like choroidal segmentation. It excels at handling class imbalance and encouraging precise pixel-wise classification, which are critical in semantic segmentation scenarios.
This makes it a superior choice for many segmentation applications, where achieving accurate pixel-level predictions is paramount. Multiple learning rates were tried but all the models favored 0.001. All the individual B-scans are then fed into the model. For each B-scan the thickness is measured along the y-axis of the image.

Each image produces an array with 684 thickness values. By composing these arrays of all the 684 images we can generate a 684 by 684 thickness map by transposing the thickness value into a color gradient where the maximum is 120px which corresponds to around 468 µm (~3.9 µm per pixel). Using a similar method an *enface* scan of vascularity can be generated. These are generated by instead of measuring the thickness, calculating the average pixel intensity in the segmented area along the y-axis. This image is not used for the classification but instead for the research purpose of aligning the maps with the ICGA scans and superimposing the generated thickness maps with ICGA scans in order to confirm the theory of Ramtohul *et al* (2023) that points of choroidal hypopermeability coincide with the thicker sections[16].

3.2.2 Dataset

The dataset used for training the segmentation models was composed using data provided by the Vitreous Macula and Retina Consultants of New York (VRMCNY) and the Nucleo Oftamologico de Almada (NOA). In total 46 individual 15mm by 15mm OCT scans from 20 patients, both healthy and with CSCR, with ages ranging from 36 to 83 from both sexes were used, with a median age of 53 years old. The following table, Table 1, contains the age and pathology distribution of the dataset collected and used in this work.

Table 1: Distribution of pathologies and sexes of the scans used in the dataset (CSCR NV: Central Serous Chorioretinopathy Neovascularized, CSCR C: Central Serous Chorioretinopathy Cronic, PN: Pachychoroid Neovascularized, PNN: Pachychoroid not vascularized).

Pathology	Male	Female
CSCR NV	2	1
CSCR C	6	2
PN	0	1
PNN	0	1
Healthy	4	3

The dataset used to train the models was composed of 120 OCT B-scans images manually segmented by specialists in ophthalmology from NOA. The validation/training split was 80%/20%.

3.2.3 Evaluation Metrics

The challenge presented can be described as a binary semantic segmentation challenge, thus the metrics used to access the performance of the segmentation models were the standard for such a challenge. In this work we measured Sorensen–Dice coefficient (more commonly referred as Dice), Recall, Pixel accuracy and Precision, described by the following formulas (TP: true positives, FP: False positives, FN: False Negatives, TN: True Negatives):

$$Dice = \frac{2 \times TP}{(TP + FP) + (TP + FN)}$$

$$Recall = \frac{TP}{TP + FN}$$

$$Pixel\ Accuraccy = \frac{TP + TN}{TP + TN + FN + FP + FN}$$

$$Precision = \frac{TP}{TP + FP}$$

3.3 Thickness Maps Classification

The second part of the pipeline consists of a binary image classification challenge. The challenge here is developing an automatic classification model that can determine, using a choroidal thickness map, if there is the existence of choroidal hyperpermeability points.

The literature on CSCR disease points to abnormal choroidal thickness and abnormal choroidal patterns are potential biomarkers of CSCR and thus also a potential indicator of choroidal hyperpermeability. Therefore, in the proposed architecture the classification model intakes the output thickness map. Using the whole OCT scan would be the optimal solution but due to the size of a scan (in average 2GB) and hardware limitations we chose to utilize thickness maps has input for the automatic classifier.

This implementation has its advantages in generating two artefacts: a classification for the presence of choroidal hyperpermeability and a thickness map, thus helping guiding physicians to a correct treatment. The image segmentation model is based on the ResNet-50 architecture and is tailored for binary image segmentation tasks. Input images are uniformly resized to 224x224 pixels to ensure consistency. The model uses a pre-trained ResNet-50 as a feature extractor, removing the original final fully connected layer. Instead, a custom linear layer is introduced with just two output units, aligning with the binary nature of the segmentation task[36]. Training this model is accomplished with the Cross-Entropy Loss function, which quantifies the disparity between predicted logits and ground truth labels assigned to each pixel in the training images. To optimize its parameters, the model employs the Adam optimizer with a learning rate of 1e-3. During training, data is divided into batches of four samples each, with shuffling for enhanced robustness. The thickness maps are images of size 684 pixels by 684 pixels RGB and for the training of the model 30 individual thickness maps were collected, 15 with the presence of choroidal hyperpermeability points and 15 without the presence of choroidal hypermobility points. In the group of “negative” choroids not only healthy choroids were included but also choroids with other pathologies but not hyperpermeability. The validation/training split was 80%/20%. To expand the dataset data augmentation techniques like flipping the image alongside the x and y axis and adding poison noise was undertaken. This resulted in having 130 images in total[37].

4. Results

The results obtained can be divided into the metrics obtained from the choroidal segmentation model, the quality of the thickness maps and the overall classification accuracy of the classification model.

4.1 Choroidal Segmentation

The following Table, Table 2, details the results when compared with the ground truth (manual segmentation by experts in the field) obtained by each model in the previously mentioned metrics. The UNET and UNET++ were both experimented with 2- and 3-layer configurations.

Due to the complexity of the problem and input size, three layered models outperformed their 2-layered counterparts.

Table 2: Choroidal Segmentation Results (%) (Dice, Acc: Pixel Accuracy, Rec: Recall, Prec: Precision)

Model	Layers	Dice	Acc	Rec	Prec
UNET	512x256x128	93.81	99.04	94.12	93.77
	512x256	90.11	96.30	91.78	91.21
UNET++	512x256x128	93.98	99.05	94.12	94.07
	512x256	90.63	96.47	91.83	91.37
DRUNET	512x256x128	94.27	99.11	94.04	94.66
SegResNet	**512x256x128**	**94.36**	**99.14**	**94.19**	**94.72**

Due to hardware limitations model size was restricted to a maximum of 3 layers. SegResNet marginally obtained the best results out of the four architectures, converging after 423 Epochs. Figure 7 represents B-scans segmented manually and by the SegResNet architecture.

4.2 Thickness Map Generation

The thickness maps were generated using the best segmentation model, SegResNet, as depicted by Table 2. The *enface* vascularity scans generated were used to align the maps with the ICGA scans. With both images superimposed our findings align with the hypothesis advanced by Ramtohul *et al* (2023) that the points of choroidal hyperpermeability coincide with the areas of abnormal thickening, as presented by Figure 8. In the acquired dataset in around 70% of the scans with choroidal hyperpermeability, the areas affected coincided with the areas of extreme thickening. Figure 8 details such cases where choroidal hypermobility coincides with the areas of abnormal thickening.

4.3 Choroidal Hyperpermeability Classification

For evaluating the classification model, a validation dataset consisting of 32 individual scans was used, 16 with choroidal hyperpermeability points (positive) and 16 without choroidal hypermobility points (negative).

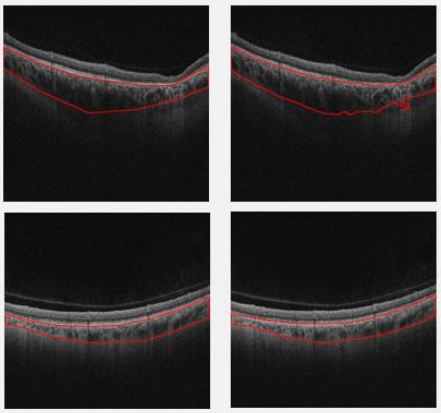

Figure 7: OCT B-scans anotated by physician (left) and anotated by automatic segmentation (right)

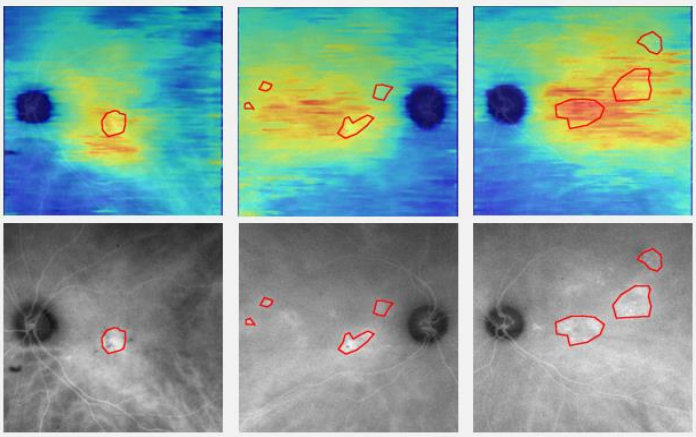

Figure 8: Thickness maps (top) and ICGA scans (bottom) with the areas of choroidal hyperpermiability anotated

Inside the negative class we used not only healthy subjects but also some patients with other pathologies like pachychoroid neovasculopathy without any presence of hyperpermeability points as well as some diabetic patients. The following graphic, Figure 9, details the results obtained by the classification model in the classification of thickness maps for the presence of choroidal hyperpermeability points.

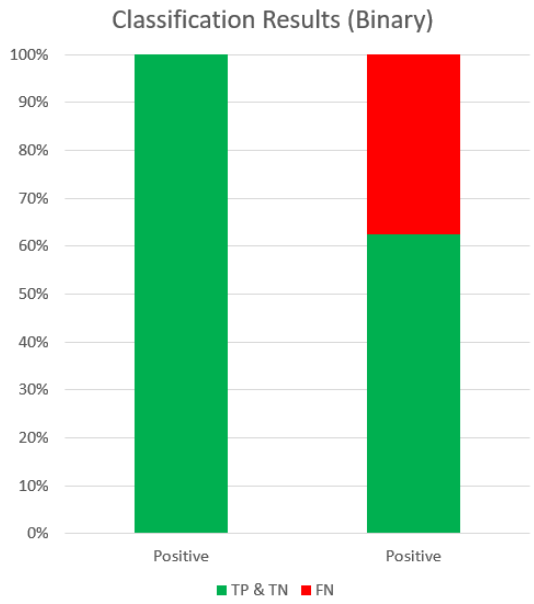

Figure 9. Classification Results with accurate predictions (TP: True Positive & TN: True Negative) marked in green and wrong predictions marked in red (FN: False Negative, with FP: False Positives = 0%)

The model accurately predicted 100% of the negative scans as being negative and accurately predicted 62,5% of positive scans as being positive. In total the overall accuracy was 81,25%, with 0% of False Positives (FP) but with 18,75% of the classifications being a False Negative.

4.4 Result Analysis

In the first section of the pipeline, the choroidal segmentation results demonstrated that the UNET architecture and its variations fit the challenge very well being able to achieve high segmentation scores. The best model (SegResNet) achieved a comparable result to the one demonstrated by Masood *et al* (2019) Kugelman *et al.* (2018) taking into consideration that the dataset size and pathologies studied differ in segmentation difficulty[33,35]. This work demonstrated that out of all the segmentation models experimented the SegResNet architecture poises itself as the most suitable architecture for the task.

The generated thickness maps generated presented a high enough quality to provide physicians with crucial information on patterns and overall areas of thickening. The quality of the thickness maps is linked to the segmentation accuracy, thus improving the accuracy would surely improve even further the quality of the maps. The maps generated when compared to the ICGA scans we had available in our dataset helped provide further evidence to the theory advanced by Ramtohul *et al* (2023) that the areas of choroidal hyperpermeability more often than not coincide with the areas of abnormal enlargement[16].

Lastly, the automatic classification results were satisfactory, the model showed a high overall accuracy in the validation set and proved extremely capable of identifying a choroid without hyperpermeability points. Nevertheless, the high number of False Negatives demonstrates that CSCR and the presence of choroidal hyperpermeability are not always linked with an extremely abnormal pattern in choroidal thickness. In those cases, the model struggled to provide an accurate enough classification, Figure 10 illustrates two cases of CSCR with choroidal hyperpermeability but one with an abnormal thickness pattern (left) and another with an even distribution of thickness (right), very similarly to what would be considered a healthy scan.

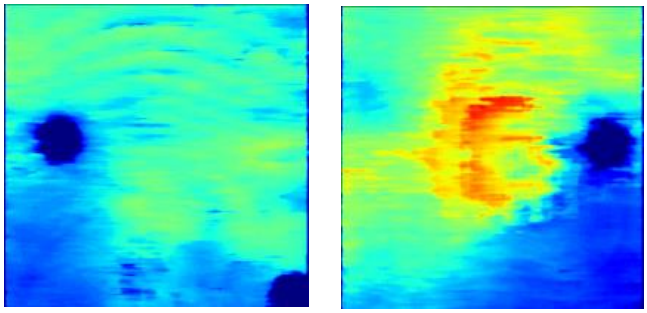

Figure 10. Two thickness maps of patients with CSCR and both with the presence of choroidal hyperpermeability confirmed by ICGA scans.

5. Conclusions & Future Improvements

In terms of choroidal segmentation, this work's findings demonstrated that in comparisson to other deep neural semantic segmentation models, the SegResNet architecture showed the best performance in all key evaluation metrics. The results fall in line with other projects in choroidal segmentation, specially given the fact that the dataset was composed with a lot of scans from older patients with pathologies where the choroid is thicker, thus harder to segmentate.

Another objective that this work achieved was to develop a pipeline that is able to generate quality thickness maps. The high segmentation quality ensured that the maps were accurate and therefore a quality extra tool for diagnosis. The generations of the thickness maps in comparison with the ICGA scans provided further confirmation of Ramtohul *et al* (2023) hypothesis that the points of choroidal hyperpermeability coincide with thickest areas of the scans.

Lastly, there were some positive takeaways from the development of automatic classification. The results obtained were very satisfactory, the model was very accurate. Nevertheless, the percentage of False Negatives and lower classification accuracy when only taking into consideration the classification of positive cases (62,5%) is a negative point. For future work, it would be a better exercise to take into consideration the 3-dimensional cube instead of working with "sliced" 2-dimensional B-scan Images. Current literature on the subject only takes into consideration working with B-scans but a more correct approach that given enough resources would surely achieve better results would be to work with the raw cubic OCT scan. This methodology would be harder to implement due to the huge size of the OCT scan but would be preferable due to the fact that when working with B-scans we loose dimensional awareness. Current methods are therefore hard-caped by that point. Our main takeaway is that it is possible to achieve a better architecture for any OCT based problem by approaching the challenge from a tridimensional approach.

With this work, we hope that new gateways for developments in the area of Artificial Intelligence applied to Ophthalmology Imaging open up leading to improvements in the quality and accessibility of diagnosis tools, thus improving patient's quality of life.

References

1. Berger, L., Bühler, V. & Yzer, S. Central Serous Chorioretinopathy - an Overview. *Klin. Monatsbl. Augenheilkd.* **238**, 971–979 (2021).
2. CHOROIDAL VASCULAR HYPERPERMEABILITY AS A PREDICTOR OF TREAT... : RETINA. https://journals.lww.com/retinajournal/Abstract/2018/08000/CHOROIDAL_VASCULAR_HYPERPERMEABILITY_AS_A.8.aspx.
3. Forrester, J. V., Dick, A. D., McMenamin, P. G., Roberts, F. & Pearlman, E. Chapter 1 - Anatomy of the eye and orbit. in *The Eye (Fourth Edition)* (eds. Forrester, J. V., Dick, A. D., McMenamin, P. G., Roberts, F. & Pearlman, E.) 1-102.e2 (W.B. Saunders, 2016). doi:10.1016/B978-0-7020-5554-6.00001-0.
4. Kaplan, H. J. Anatomy and function of the eye. *Chem. Immunol. Allergy* **92**, 4–10 (2007).
5. Nguyen, K. H., Patel, B. C. & Tadi, P. Anatomy, Head and Neck: Eye Retina. in *StatPearls* (StatPearls Publishing, 2023).
6. Posterior Eye Segment - an overview | ScienceDirect Topics. https://www.sciencedirect.com/topics/immunology-and-microbiology/posterior-eye-segment.
7. BS, M. A. Z., PhD, and Philip J. Luthert, BSc, MB & Specialist, R. The Choroid in AMD: A Critical Point of Failure? http://www.retina-specialist.com/article/the-choroid-in-amd-a-critical-point-of-failure-1.
8. Caceres, P. S. & Rodriguez-Boulan, E. Retinal pigment epithelium polarity in health and blinding diseases. *Curr. Opin. Cell Biol.* **62**, 37–45 (2020).
9. Kaye, R. *et al.* Central serous chorioretinopathy: An update on risk factors, pathophysiology and imaging modalities. *Prog. Retin. Eye Res.* **79**, 100865 (2020).

10. Chen, G. *et al.* Subfoveal Choroidal Thickness in Central Serous Chorioretinopathy: A Meta-Analysis. *PLoS ONE* **12**, e0169152 (2017).
11. Hiroe, T. & Kishi, S. Dilatation of Asymmetric Vortex Vein in Central Serous Chorioretinopathy. *Ophthalmol. Retina* **2**, 152–161 (2018).
12. Ota, T. *et al.* Subfoveal serous retinal detachment associated with extramacular branch retinal vein occlusion. *Clin. Ophthalmol. Auckl. NZ* **7**, 237–41 (2013).
13. Reinhart, M. B., Huntington, C. R., Blair, L. J., Heniford, B. T. & Augenstein, V. A. Indocyanine Green: Historical Context, Current Applications, and Future Considerations. *Surg. Innov.* **23**, 166–175 (2016).
14. Lim, J. I. & Flower, R. W. Indocyanine green angiography. *Int. Ophthalmol. Clin.* **35**, 59–70 (1995).
15. Pang, C. E., Shah, V. P., Sarraf, D. & Freund, K. B. Ultra-Widefield Imaging With Autofluorescence and Indocyanine Green Angiography in Central Serous Chorioretinopathy. *Am. J. Ophthalmol.* **158**, 362-371.e2 (2014).
16. Ramtohul, P., Cabral, D., Oh, D., Galhoz, D. & Freund, K. B. En face Ultrawidefield OCT of the Vortex Vein System in Central Serous Chorioretinopathy. *Ophthalmol. Retina* **7**, 346–353 (2023).
17. Indocyanine Green Angiography | Department of Ophthalmology. https://ophthalmology.med.ubc.ca/patient-care/ophthalmic-photography/indocyanine-green-angiography/.
18. Spaide, R. F., Fujimoto, J. G., Waheed, N. K., Sadda, S. R. & Staurenghi, G. Optical coherence tomography angiography. *Prog. Retin. Eye Res.* **64**, 1–55 (2018).
19. Podoleanu, A. G. Optical coherence tomography. *J. Microsc.* **247**, 209–219 (2012).
20. Aumann, S., Donner, S., Fischer, J. & Müller, F. Optical Coherence Tomography (OCT): Principle and Technical Realization. in *High Resolution Imaging in Microscopy and Ophthalmology: New Frontiers in Biomedical Optics* (ed. Bille, J. F.) 59–85 (Springer International Publishing, 2019). doi:10.1007/978-3-030-16638-0_3.
21. Guo, Y., Liu, Y., Georgiou, T. & Lew, M. S. A review of semantic segmentation using deep neural networks. *Int. J. Multimed. Inf. Retr.* **7**, 87–93 (2018).
22. Understanding of a convolutional neural network | IEEE Conference Publication | IEEE Xplore. https://ieeexplore.ieee.org/abstract/document/8308186.
23. Brownlee, J. What is the Difference Between a Batch and an Epoch in a Neural Network?
24. Ruder, S. An overview of gradient descent optimization algorithms. Preprint at https://doi.org/10.48550/arXiv.1609.04747 (2017).
25. Janocha, K. & Czarnecki, W. M. On Loss Functions for Deep Neural Networks in Classification. Preprint at https://doi.org/10.48550/arXiv.1702.05659 (2017).
26. Soulami, K. B., Kaabouch, N., Saidi, M. N. & Tamtaoui, A. Breast cancer: One-stage automated detection, segmentation, and classification of digital mammograms using UNet model based-semantic segmentation. *Biomed. Signal Process. Control* **66**, 102481 (2021).
27. Ballestar, L. M. & Vilaplana, V. MRI Brain Tumor Segmentation and Uncertainty Estimation Using 3D-UNet Architectures. in *Brainlesion: Glioma, Multiple Sclerosis, Stroke and Traumatic Brain Injuries* (eds. Crimi, A. & Bakas, S.) 376–390 (Springer International Publishing, 2021). doi:10.1007/978-3-030-72084-1_34.
28. Zhou, Z., Rahman Siddiquee, M. M., Tajbakhsh, N. & Liang, J. UNet++: A Nested U-Net Architecture for Medical Image Segmentation. in *Deep Learning in Medical Image Analysis and Multimodal Learning for Clinical Decision Support* (eds. Stoyanov, D. et al.) 3–11 (Springer International Publishing, 2018). doi:10.1007/978-3-030-00889-5_1.
29. Tsang, S.-H. Review: UNet++ — A Nested U-Net Architecture (Biomedical Image Segmentation). *Medium* https://sh-tsang.medium.com/review-unet-a-nested-u-net-architecture-biomedical-image-segmentation-57be56859b20 (2019).
30. Devalla, S. K. *et al.* DRUNET: a dilated-residual U-Net deep learning network to segment optic nerve head tissues in optical coherence tomography images. *Biomed. Opt. Express* **9**, 3244–3265 (2018).

31. Myronenko, A. 3D MRI Brain Tumor Segmentation Using Autoencoder Regularization. in *Brainlesion: Glioma, Multiple Sclerosis, Stroke and Traumatic Brain Injuries* (eds. Crimi, A. et al.) 311–320 (Springer International Publishing, 2019). doi:10.1007/978-3-030-11726-9_28.
32. Wang, L. *et al.* Comparative analysis of image classification methods for automatic diagnosis of ophthalmic images. *Sci. Rep.* **7**, 41545 (2017).
33. Masood, S. *et al.* Automatic Choroid Layer Segmentation from Optical Coherence Tomography Images Using Deep Learning. *Sci. Rep.* **9**, 3058 (2019).
34. Abouelnaga, Y., Ali, O. S., Rady, H. & Moustafa, M. CIFAR-10: KNN-Based Ensemble of Classifiers. in *2016 International Conference on Computational Science and Computational Intelligence (CSCI)* 1192–1195 (2016). doi:10.1109/CSCI.2016.0225.
35. Kugelman, J. *et al.* Automatic choroidal segmentation in OCT images using supervised deep learning methods. *Sci. Rep.* **9**, 13298 (2019).
36. He, K., Zhang, X., Ren, S. & Sun, J. Deep Residual Learning for Image Recognition. Preprint at https://doi.org/10.48550/arXiv.1512.03385 (2015).
37. Akbiyik, M. E. Data Augmentation in Training CNNs: Injecting Noise to Images. (2019).